ACS APPLIED MATERIALS & INTERFACES
Research Article
www.acsami.org

Huge Photoresistance in Transparent and Conductive Indium Titanium Oxide Films Prepared by Electron Beam−Physical Vapor Deposition

Rocío Martínez-Morillas,[†] Rafael Ramírez,[‡] Jorge Sánchez-Marcos,[†,#] Emiliano Fonda,[§] Alicia de Andrés,[†] and Carlos Prieto*[,†]

[†]Instituto de Ciencia de Materiales de Madrid, Consejo Superior de Investigaciones Científicas, Cantoblanco, 28049 Madrid, Spain
[‡]Departamento de Física, Escuela Politécnica Superior, Universidad Carlos III de Madrid, Avenida Universidad 30, Leganés, 28911 Madrid, Spain
[#]Departamento de Química-Física Aplicada, Universidad Autónoma de Madrid, Cantoblanco, 28049 Madrid, Spain
[§]Synchrotron SOLEIL, F-91192 Gif Sur Yvette, France

Supporting Information

ABSTRACT: Transparent and conductive indium titanium oxide (ITiO) films have been obtained by electron beam physical vapour deposition with Ti content from 5 at % up to 28 at %. X-ray absorption spectroscopy techniques have been used to identify the local environment of Ti ions. Even at the lowest concentrations Ti is not incorporated into the In_2O_3 structure but forms clusters of a Ti−In mixed oxide that present a distorted rutile TiO_2 short-range order. The optical transmittance of the annealed samples reaches 95 % and no significant variation of the gap energy (around 3.7 eV) is observed with Ti content. The electronic conductivity under light irradiation is studied evidencing a huge photo-resistance in the samples with Ti content above 22 at % reaching more than two orders of magnitude for the 26 at % Ti under illumination with few μW/cm^2 at 365 nm. Hall and conductivity results are analyzed using a model that takes into account both electron and hole carriers as well as the conductivity enhancement by carrier photogeneration. The electron carrier density decreases with Ti content while its mobility increases up to values of 1000 cm^2/(V s). Oxygen annealed ITiO films obtained by this technique with Ti content below 10 at % have properties adequate as transparent semiconductors and those with Ti content higher than 22 at % have exceptional photoresistive properties relevant for numerous applications.

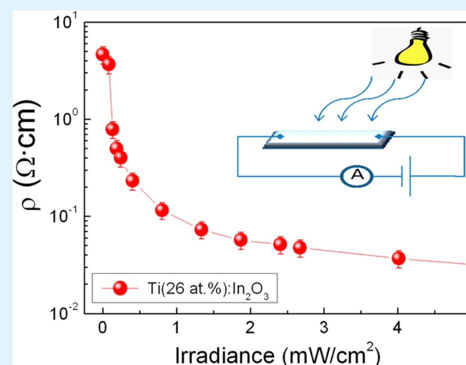

KEYWORDS: *transparent conductive materials, photoresistance*

1. INTRODUCTION

Research on transparent conducting materials (TCM) may be considered as the key for full development of a large number of new technological devices such as flat-panel displays, electroluminescent devices, photovoltaic cells, light emitting diodes, and all-purpose smart windows.[1] Although indium tin oxide (ITO) is the most commonly used electrode,[2] a large list of different TCMs provides improved properties for demanding applications. In this sense, the use of transparent electrodes in devices using wide band gap semiconductors requires a special attention to electron mobility and carrier density. Typically, high electron mobility and low carrier concentration are directly linked with the enhancement of the optical transmission at the red and infrared wavelength regions without lowering electrical conductivity.

Indium molybdenum, indium tungsten, and indium titanium oxides (IMO, IWO, and ITiO, respectively) thin films present transparent conductive properties with low electrical resistivity and high mobility.[3,4] Specifically, ITiO has been recently reported to have an excellent electronic mobility for Ti content below 5 at %.[5] This system has been prepared by different methods: pulsed laser deposition,[6] magnetic null discharge sputter source[7] or by sputtering from ceramic targets[8] and recently by electron beam physical vapor deposition[9] (EB-PVD). In all of them, conductive samples are obtained for Ti contents lower than 20 at %.

Additionally, the doping of ITO with titanium has been reported to extend its electrode utility to active materials in transparent field-effect transistors,[10] which makes of particular importance the reactivity between In oxides and TiO_2.[11]

In this work, we report on the characterization of ITiO films prepared from In_2O_3−TiO_2 blends by EB-PVD. The study has been conducted on a set of films prepared over a wide Ti-content range (up to nearly 30%). Before the standard optical

Received: October 29, 2013
Accepted: January 15, 2014
Published: January 15, 2014

ACS Publications © 2014 American Chemical Society

and electrical characterization (to determine transparency and resistivity), the local Ti environment has been studied by X-ray absorption spectroscopy (XAS) synchrotron techniques. Finally, it is reported a new interesting effect: films with near 30 at % Ti-content exhibit an important photoresistance (PR) effect with a resistivity decrease of several orders of magnitude under moderate light irradiance.

Photoresistivity has several important applications as bistable optical switches[12,13] and radiation detectors[14,15] and in the case of TiO_2, it becomes of fundamental interest for photoelectrochemical solar cells and photocatalytic reactors for pollution control.[16] The PR effect has been reported in ZnO and TiO_2 polycrystalline systems[17,18] and in ZnO single-crystal[19] wide band gap semiconductors. Such variation of resistivity upon light illumination is often referred as persistent photoresistivity. In nanocrystalline TiO_2 thin films, the mechanism for the PR has been attributed to electron and hole spatial separation because of excess-charge-dependent potential barriers at interfaces between grains boundaries and to inhomogeneities.[20]

2. EXPERIMENTAL SECTION

ITiO films were deposited by using a 6 kW electron beam source (EVM-6 from Ferrotec GmbH) placed in a standard PLS-500 Pfeiffer vacuum chamber equipped with a secondary load-lock chamber. The source was operated with a GENIUS evaporation controller with a CARRERA high voltage power supply. The vacuum system provides a base vacuum in the range of 1×10^{-7} mbar and typical pressures about 1×10^{-5} mbar during deposition.

Starting targets are formed by rutile-TiO_2 and In_2TiO_5, they were sintered as low density ceramics pellets by heating at 1200 °C for 2 h Ti-rich blends of TiO_2 and In_2O_3 (from Aldrich) previously pressed (uniaxially near 10 Pa) at room temperature. The main parameters for EB-PVD preparation were: electron-beam acceleration voltage of 6 kV and electron-beam current intensity of 20 mA. Depending on the target composition, those parameters allow deposition rates ranging from 1 to 10 nm/min. For this study, films with thicknesses in the 50−200 nm range were deposited on non-intentionally heated Si(100) of very high resistivity and on fused quartz substrates to be used, respectively, for electrical and optical characterizations. This paper reports on as-deposited films as well as on O_2-annealed films. The annealing process consisted in heating the samples during 24 h at 500 °C in a furnace within a quartz tube previously evacuated to a residual vacuum of 1×10^{-6} mbar, later on, oxygen flows at a pressure of 1×10^{-2} mbar during warming up, constant temperature annealing and cooling down steps.

The Ti/In ratio was determined by analyzing the energy dispersive X-ray fluorescence (EDX) with an EDAX Genesis XM2i analyzer coupled to a FEI NanoSEM Nova 230 field emission-scanning electron microscope (FE-SEM).

The film thickness was determined by X-ray reflectivity carried-out with a Bruker D-8 diffractometer working with the Cu K_α wavelength. Also, atomic force microscopy was used to measure film thickness of step-masked samples and to test the film surface homogeneity (see the Supporting Information, Figure S1). Moreover, optical pictures of the samples and micrograph images are reported in Figure S1 to show the quality and transparence of the films.

X-ray diffraction characterization was carried out at the BM25-Spline Spanish beamline of the European Synchrotron Radiation Facilities (ESRF). X-ray absorption near-edge spectroscopy (XANES) and extended X-ray absorption fine structure (EXAFS) spectroscopies at the Ti K-edge were measured at 40 K in the fluorescence yield mode at the SAMBA beamline of the French Synchrotron Radiation Facility (SOLEIL).

EXAFS analysis was performed using the VIPER software,[21] by following the procedure described in the Supporting Information. The amplitude and phase functions introduced as inputs in the analysis were obtained by the FEFF8 code.[22,23]

The optical absorption of the samples grown on fussed silica has been characterized with a Cary 4000 UV−vis spectrophotometer in the 190−900 nm ultraviolet−visible (UV−vis) range. The electrical properties were obtained with a Keithley 2400 Source-Meter and a Keithley 2000 digital voltmeter managed by a home-made computer software to quantify $I-V$ and $V-H$ curves. Hall effect measurements were made at room temperature by placing samples in a variable magnetic field provided by a standard electromagnet (-0.8 T < H < 0.8 T). According with the van der Pauw method,[24] four silver paint contacts, over aluminum electrodes previously deposited by sputtering through a mask, were placed on the film surface corners of squared samples grown on highly resistive Si (001) wafers. It should be commented that no differences have been observed when silver paint was used directly on ITiO films.

3. RESULTS AND DISCUSSION

The Ti-content in the films prepared by this EB-PVD preparation technique are considerably lower compared to the values in the starting pellet.[9] Therefore, the starting pellets were made with very high Ti-content (up to nearly 95 at %) and, consequently, the evaluation of the Ti content of each studied film was necessary. The Ti content in the films was evaluated by EDX analysis and additionally confirmed by Rutherford backscattering spectroscopy (RBS).

Thin films with Ti content as high as 30 at % have been successfully obtained with remarkable properties and the added interest of the reduced indium content (where the Ti content has been calculated as $C_{Ti} = [Ti]/([Ti] + [In])$). Among a set of films with Ti content in the 4−30 at % range, five representative samples with C_{Ti} = 5, 8, 22, 26, and 28 at % have been selected for the here presented study.

X-ray diffraction (XRD) data of two O_2-annealed characteristic samples are given in Figure 1a. In_2O_3 crystallizes in the cubic $Ia\bar{3}$ space group, which may be seen as a fluorite-related superstructure[25] where one-fourth of the oxygen atoms are missing and indium atoms are located at six-fold coordinated sites. That structure fits the C_{Ti} = 8 at % film, but no diffraction peaks are found in the C_{Ti} = 26 at % film. By using the Rietveld method,[26] a small change has been detected (0.4 %) in the lattice parameter (a=10.085(1) for the C_{Ti} = 8 at % film compared to that reported for powder In_2O_3 (a = 10.1192(2)).[27] Low doped "O_2-annealed" ITiO films with C_{Ti} < 10 at % have the long-range-order imposed by the In_2O_3 cubic structure, but films with C_{Ti} > 20 at % show an amorphous or nanocrystalline character. In order to address the important question of the Ti local environment, we have carried out Synchrotron Radiation X-ray absorption experiments at the Ti K-edge. This technique provides information by two independent ways: XANES is related to oxidation state and stereo-chemical coordination of the absorbing atoms and, on the other hand, EXAFS gives information on the radial distribution of distances and neighbors around the absorber.

On the other hand, using density-functional first principles calculations, In-doped rutile and Nb- doped anatase TiO_2 structures have been predicted to be TCM.[28,29] In this rutile $Ti_{1-x}In_xO_2$ structure, titanium is located at octahedral six-fold coordinated sites, with four Ti−O distances at 1.94 Å and two other at 1.97 Å, and the first Ti−Ti coordination sphere comprises 10 atoms: two of them at 2.93 Å and eight more at 3.55 Å.

The K-edge XANES of non-centrosymmetric Ti oxides is characterized by a pronounced peak before the main rising edge

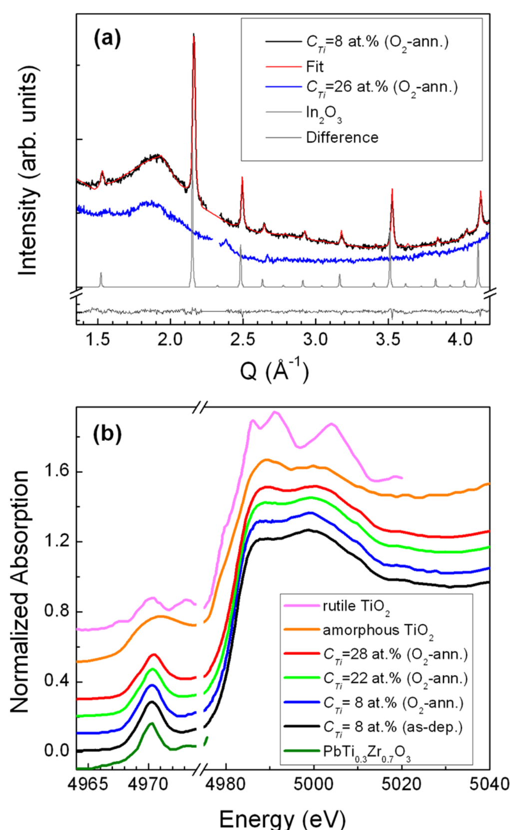

Figure 1. (a) XRD spectra of two representative O_2-annealed ITiO films; the diffraction pattern of the In_2O_3 cubic structure, the fit and the difference are also given. (b) XANES spectra at the Ti K-edge of selected ITiO films (note the break in the energy axis to observe the pre-peak details.

related to a transition from the 1s to unoccupied 3d electronic states. This dipole forbidden electronic transition becomes allowed by the mixture of the p character of the surrounding oxygen atoms and the unfilled 3d Ti states, its intensity is proportional to the square of the distortion of the centrosymmetry structure.[30−32]

Figure 1b shows the XANES spectra of some representative ITiO films. The spectra clearly correspond to the Ti^{4+} oxidation state and no appreciable differences are obtained along the series indicating that titanium has a similar environment in all samples. The films with C_{Ti} = 8 at % are representative to evaluate the influence of oxygen annealing on the whole set of samples. The measurements indicate that annealing in oxygen atmosphere has no influence on the short-range order, showing that no re-accommodation of Ti ions is promoted. On the other hand, no differences are appreciable between the spectra corresponding to the O_2-annealed films (C_{Ti} = 8, 22, and 28 at %), indicating that, for the studied Ti-content range, the observed short range order around Ti ions does not depend on its concentration in the film. The resonances above the edge, which are related with the medium-range structure, in all ITiO films are similar to that observed in amorphous or nanocrystalline phases of TiO_2.[33]

Conversely, the pre-peak of the ITiO films is clearly different to that obtained for amorphous TiO_2 and the shape is slightly different to that corresponding to rutile. Titanium perovskites are excellent reference compounds to obtain information from this pre-peak. Looking at the 1s−3d electronic transitions, Ti in TiO_6 octahedra provides characteristic pre-peaks which allow distinguishing, independently of its crystallographic long-range order, between centrosymmetric distortion (as in $EuTiO_3$ or $CaTiO_3$), close to centrosymmetric (as in $SrTiO_3$), tetragonal (as in $PbTi_xZr_{1-x}O_3$ independently of Ti concentration), or rhombohedral distortion (as in $BaTiO_3$).[30] For comparison purposes, Figure 1b shows also the pre-peak of $PbTi_{0.3}Zr_{0.7}O_3$,[30] the excellent similarity with the intensity and shape of the obtained pre-peak in ITiO films proves that titanium is enclosed in TiO_6 octahedra with a tetragonal distortion. The joint information from pre-peak and from the resonances above the edge points towards, independently of the annealing and of the Ti content, Ti present in ITiO films forming a TiO_2-related structure with tetragonally distorted TiO_6 octahedra and disorder at the medium-range distances.

No strong variation is observed in the radial distribution function around Ti atoms, neither with the Ti content nor after annealing (see Figure S2 in the Supporting Information). EXAFS analysis of the second peak of the Fourier transform may give significant information of the phase in which Ti appears, but similarly to the studies reported[27,34] for ITO, its magnitude is very small. The fit of the first peak (at ∼1.5 Å in the FT magnitude) of all samples indicates the presence of six Ti−O neighbors at $R_1 \approx 1.9$ Å (the fited distances, number of neighbors, and Debye−Waller factor values are summarized in Table S1 in the Supporting Information). In the fit of the second peak (at ∼3 Å in the FT magnitude), distances around 2.9 and 3.0 Å are obtained for Ti−In and Ti−Ti pairs, respectively. The observed small magnitude is obtained by the destructive interference from these Ti−In and Ti−Ti contributions. The obtained distances and number of neighbors are compatible with those in the rutile structure where a slight distortion due to the inclusion of indium atoms can be expected.

In summary for all the studied samples, the EXAFS analysis indicates that the first Ti- coordination sphere is formed by oxygen octahedra and that the second neighbor distances are compatible with a distorted rutile structure of a double Ti−In oxide. This picture is in agreement with XANES, which shows that the tetragonal environment of Ti is slightly different from that in rutile. XRD indicates that the long-range order of the In_2O_3 structure (observed at low Ti doping) disappears at high Ti content, consistent with the formation of a nanosized double Ti−In oxide.

From the optical point of view, the transparency of as-deposited films strongly depends on the titanium content. The films with low Ti content (C_{Ti} < 10 at %) have a grey metallic aspect while samples with high Ti-content (C_{Ti} > 10 at %) appear transparent. For instance, films of C_{Ti} = 22 at % and thickness of 82 nm have a transmittance of 86%. The absorption coefficient (α) was obtained using the measured film thickness. Figure 2 shows the optical absorption spectra of as-deposited and O_2-annealed films. "As-deposited" films are transparent in the visible range only for Ti content higher than 20 at %. On the other hand, the whole set of samples becomes transparent after O_2-annealing. The low transparency is commonly attributed to oxygen vacancies in the as-deposited films, which are filled when oxygen is supplied at high temperatures.

The optical absorption edge of In_2O_3 is described by a direct allowed transition, with $n = 1/2$ in the Tauc expression[35] for the optical absorption as a function of the light energy ($h\nu$) and the band-gap (E_g):

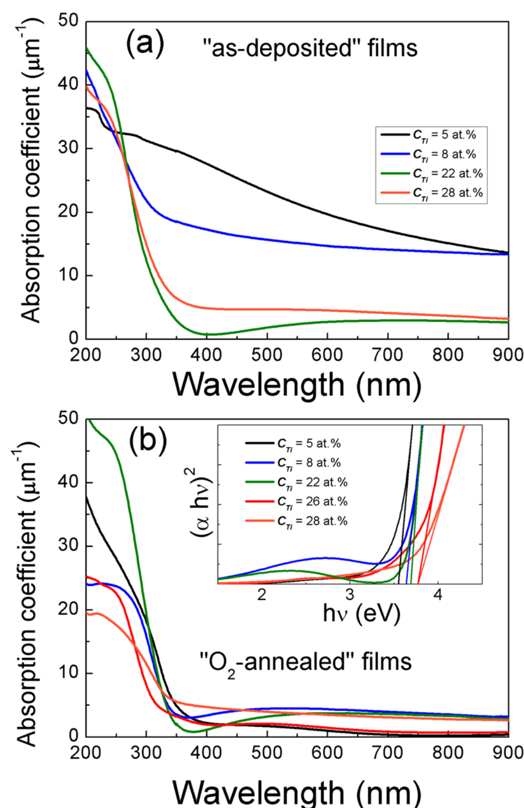

Figure 2. Wavelength dependence of the absorption coefficient: (a) as-deposited, (b) O_2-annealed ITiO films. Inset shows the representation for band gap determination.

$$\alpha h\upsilon \propto (h\upsilon - E_g)^n \quad (1)$$

The inset of Figure 2b shows the representation required to determine the band-gap energy of each sample. The obtained values are in the 3.6−3.8 eV range, close to the reported value[36] for In_2O_3 and not far from that of TiO_2.[37] It may be noted that even if an increasing trend with the Ti content seems to be present, the variation is similar in magnitude to the experimental error mainly because of the presence of oscillations in the spectra related to the film thickness.

In the present study, the electrical resistivity has been carefully determined by the four points van der Pauw method[24] for both sets of samples (as-deposited and O_2-annealed). Figure 3 shows the obtained values and the dependence of electrical resistivity as a function of the Ti content.

Resistivity presents acceptable values for the as-deposited films with less than 10 at % Ti content, but they have to be discarded for applications because of their strong optical absorption. Nevertheless, as-deposited films with Ti-content near 20 at % show acceptable optical transmittance (∼94 % at 500 nm) and resistivity values of 1.9×10^{-2} Ω cm (sheet resistance ∼2.3×10^3 Ω for a film of 82 nm thick). This resistivity value is nearly one order of magnitude higher than the best ones reported when deposited by PLD or sputtering,[6,38] but it should be taken into account that for the here reported as-deposited films, no optimization of the deposition temperature was made.

The O_2-annealed series shows a similar behavior, in which the resistivity is nearly one order of magnitude larger than for the as-deposited films. In conclusion, O_2-annealing promotes higher transparency, but worse electrical conductivity of ITiO films.

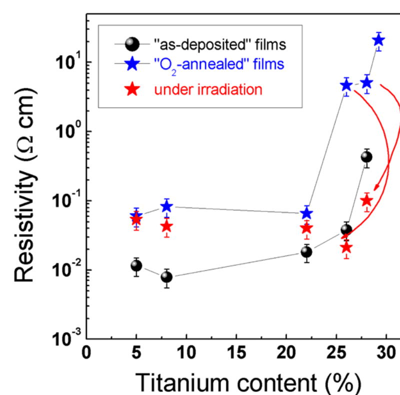

Figure 3. Dark resistivity obtained for as-deposited (spheres) and O_2-annealed (blue stars) ITiO films vs. the Ti content defined by C_{Ti} = [Ti]/([Ti] + [In]). Resistivity values obtained under irradiation of O_2-annealed ITiO films are also showed (red stars).

The most remarkable aspect of the O_2-annealed samples with Ti content above 22 at % is the huge reduction of resistivity under moderate irradiation with visible light. This property is of paramount interest for singular applications as in bistable optical switches. Figures 4−6 show the effect of light intensity on the electrical transport for samples with different Ti content. For this purpose, constant temperature electrical measurements have been performed at 300 K under light irradiation obtained from a cold source based on a halogen lamp guided through an optical fiber in order to cut wavelengths in the infrared region (its spectrum is shown in Figure S3 of the Supporting Information).

Figure 4 shows raw van der Pauw measurements under different white visible light irradiation power. The samples with Ti content higher than 22 at % exhibit strong variation of resistivity, which is clearly not the case for films with low Ti content. Figure 5a depicts the obtained resistivity as a function of the irradiation intensity. It should be highlighted that, under illumination, a resistivity variation of more than two orders of magnitude is obtained in the C_{Ti} = 26 at % film (the obtained values under irradiation are also plotted in Figure 3). On the other hand, it is worth noting that the major variation is obtained in the 0−1 mW/cm^2 irradiation range that should be compared with the value of 0.1 mW/cm^2, which is a typical lower value for room lighting. Additionally, sample heating by the incident light can be discarded as the origin of the change in resistivity because, for instance, we have observed that C_{Ti} = 26 at % sample needs an increase of more than 100 °C from room temperature to show a resistivity variation of two orders of magnitude.

The spectral dependence of the photoresistance was measured under monochromatic irradiation using the spectral lines of a mercury-vapor lamp. Figure 5b shows the obtained resistivity as a function of the irradiation energy. Even if the observed variation is stronger for UV wavelengths, the obtained variation is similar to the effect observed under white irradiation, only C_{Ti} = 26 at % and C_{Ti} = 28 at % samples show a remarkable decrease of resistivity. It should be noted that the photon energies of all used monochromatic lines are lower than the optical gap but, in fact, below the absorption edge, a tail can be observed in the absorption coefficient of the films (Figure 5b), which is characteristic of polycrystalline

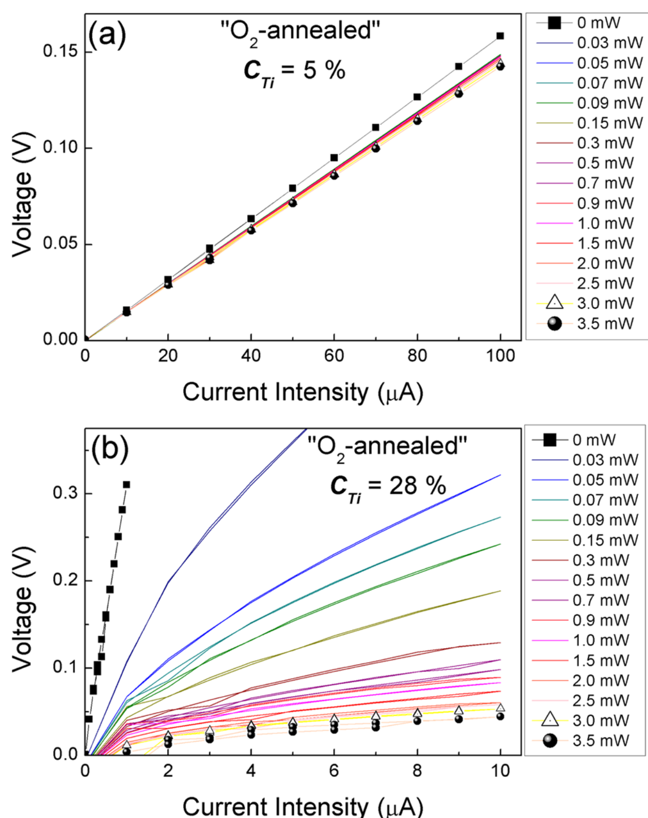

Figure 4. Van der Pauw $I-V$ curves under white light irradiation for two characteristic samples. (a) C_{Ti} = 5 at % film. (b) C_{Ti} = 28 at % film. In both cases, from darkness (full squares) to 3.5 mW (circles).

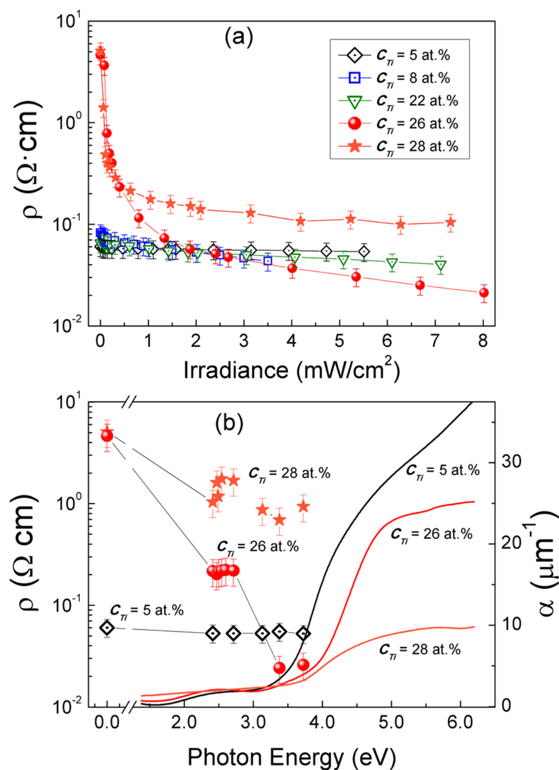

Figure 5. (a) Resistivity vs. white light irradiance. (b) Resistivity obtained under different monochromatic light irradiation in comparison with the optical absorption spectra.

materials.[39] This so-called Urbach tail is described by a distribution of indirect transitions that allows a $\alpha h\upsilon \propto (h\upsilon - E_g)^2$ dependence,[40] but this function gives a poor fit of our ITiO films. Conversely, and in a parallel way to what is observed for CdSe films,[41] the absorption tail of ITiO films well fits the expression

$$\alpha = \mathrm{B}e^{(h\upsilon - E_g)/\Gamma} \qquad (2)$$

where Γ is a parameter that increases with the structural disorder of the material.[42] The best fits for C_{Ti} = 5, 26, and 28 at % samples give, respectively, Γ values of 0.62, 2.55, and 2.88 eV, in agreement with the expected increase due to the In_2O_3 crystallinity worsening because of the higher Ti content.

Key parameters for transparent electrodes are carrier density and mobility. In this case, their dependence with irradiance should be analyzed. For that purpose, the Hall voltage has been measured at room temperature as a function of magnetic field for a constant current intensity of 50 μA (Figure 6). ITiO films with of C_{Ti} = 5 and 8 at % do not have appreciable variation in the Hall resistance, but samples with Ti content higher than 20 at % show a variation of the Hall voltage slope indicating a change of the carrier density under irradiance.

The Hall coefficient, which is proportional to the slope, has a mixed behavior as light power increases; in particular, for C_{Ti} = 26 and 28 at % samples, this coefficient decreases with increasing light power while for C_{Ti} = 22% at % sample, the opposite trend is observed. Another interesting feature is that C_{Ti} = 26 at % sample shows a change in the sign of the Hall coefficient at very low level of illumination: It is positive for the measurement in nearly darkness conditions (accounting for positive charge hole carriers) and changes to negative under illumination (accounting for electron carriers). These facts indicate the presence of both types of carriers. As shown in the Supporting Information, the change in the sign of the slope can be explained assuming that conductivity is due to different, but non-negligible, carrier concentration of electrons and holes.[43]

After considering the presence of electron and holes, the density and mobility of both types of carrier can be estimated under reasonable assumptions (see the Supporting Information). In Figure 7, the obtained dark electron concentration and electron mobility are plotted against the sample Ti content. Since sample preparation is not intended to obtain excellent values of resistivity, the obtained carrier densities are quite small. Nevertheless, the mobility obtained for the samples with low Ti-content (145 and 160 $cm^2/(V\ s)$ for C_{Ti} = 5 and 8 at %, respectively) have similar values as those reported for similar titanium doping level by several authors in the literature, where mobilities of 50 and 100 $cm^2/(V\ s)$ have been reported for films with 1 wt %,[5,44] and 83 and 159 $cm^2/(V\ s)$ for Ti contents of 6 at % and 5 wt %,[6,8] respectively. More interesting is the large increase of the mobility obtained for the samples with Ti content above 20 at %, which becomes increased by one order of magnitude, arriving at nearly 1000 $cm^2/(V\ s)$.

Comparing with the more studied ITO system, at a first sight, mobility of samples with low Ti content (140 $cm^2\ V^{-1}\ s^{-1}$) may look too high compared to the typical 40 $cm^2\ V^{-1}\ s^{-1}$ value of ITO films[45] or even with 65 $cm^2\ V^{-1}\ s^{-1}$ obtained for transparent ITO nanowires[46] used in field-effect transistors.[47] However, as a general trend empirically observed for a large number of semiconductors,[48] mobility is expected to rise as donor concentration diminishes. In this sense, the O_2-annealing process has provided excellent transparent ITiO films with very low donor concentrations and high mobility, which becomes

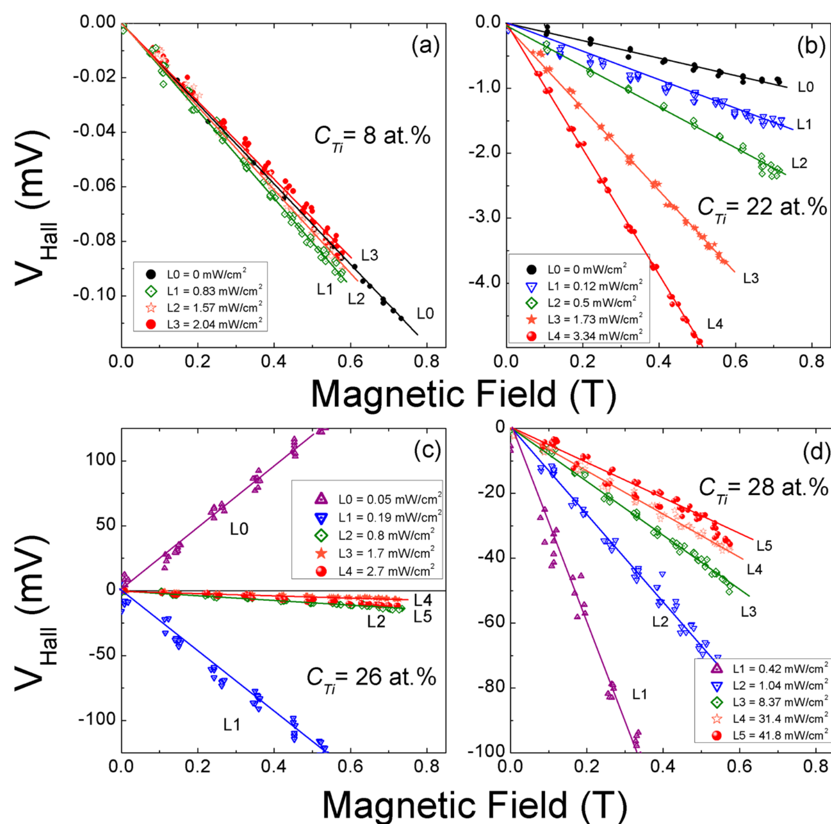

Figure 6. Hall voltage obtained under several irradiances for different films: (a) C_{Ti} = 8 at %, (b) C_{Ti} = 22 at %, (c) C_{Ti} = 26 at %, (d) C_{Ti} = 28 at %.

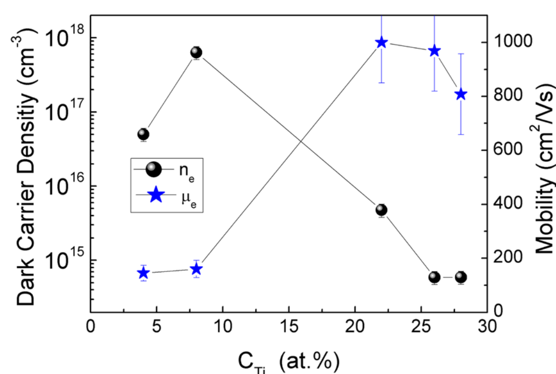

Figure 7. Dark carrier density and mobility obtained for samples with different Ti content.

especially significant for films in the 20−30 at % Ti-content range that presents the highest reported mobility values (near 1000 $cm^2/(V\ s)$) in these indium oxide TCM system.

Finally, because the here reported ITiO films present TiO_2 segregation in a TCM system, a deep study have to be done in this ITiO system to be compared, for instance, with nanoparticulate TCM coated by a TiO_2 shell. Such kind of electrodes, have been proposed for the enhancement of electron extraction in dye-sensitized solar cells. In these cells, electrodes made from structures formed by the conductive fluorinated SnO_2 covered by TiO_2 are reported to reduce the electron transit time without increasing the recombination resistance,[49] or TiO_2 coating prepared by atomic layer deposition on mesoporous SiO_2 templates to obtain high conversion efficiency.[50]

4. CONCLUSIONS

EB-PVD has been used to prepare transparent and conductive ITiO films with Ti content up to nearly 30 at %. X-ray absorption techniques have been used to study the short range order of Ti ions, independently of the Ti content from 5 to 28 at %, results show that they are not incorporated into the In_2O_3 structure but they are forming a distorted rutile structure of a double Ti−In oxide.

Annealed films show an optical transmittance of 95% with no significant variation of the gap energy (around 3.7 eV) with Ti content and resistivity in the range of 1×10^{-2} Ωcm. Films with Ti-content in the range of 26−28 at % have much more higher resistivity (∼1 Ω cm) at darkness and, additionally, they show a photoresistivity effect of two orders of magnitude under moderate white light irradiance, as well as under only a few $\mu W/cm^2$ at 365 nm. Conductive properties have been analyzed by taking into account the presence, as well as the photogeneration of electron and holes as charge carriers. In this sense, the film with Ti content of 26 at % shows p-type dominant charge carrier in darkness, which can be switched to n-type for low-level light irradiation.

Results for ITiO films with 5−8 at % Ti content allow mobility (∼100 cm/(V s)) slightly higher than that reported for indium tin oxide, and films with Ti content higher than 20 at % present an enhancement of one order of magnitude of its mobility values (∼1000 cm/(V s)), which make ITiO films the indium-oxide-based TCM with the highest reported mobility.

■ ASSOCIATED CONTENT

Supporting Information

Additional figures, tables, and information (PDF). This material is available free of charge via the Internet at http://pubs.acs.org.

dx.doi.org/10.1021/am404675n | ACS Appl. Mater. Interfaces 2014, 6, 1781−1787

AUTHOR INFORMATION

Corresponding Author

*E-mail: cprieto@icmm.csic.es.

Notes

The authors declare no competing financial interest.

ACKNOWLEDGMENTS

We acknowledge financial support to Spanish MICINN and MINECO though contracts MAT2009-08786 and MAT2012-37276-C03-01 and to the Madrid regional government though Contract S2009/MAT-1756. In addition, assistance from SAMBA beamline staff at SOLEIL and from Spline at ESRF is acknowledged.

REFERENCES

(1) Hartnagel, H. L.; Dawar, A. L.; Jain, A. K.; Jadadish, C. *Semiconducting Transparent Thin Films*; Institute of Physics: Bristol, U.K., 1995; pp 1−358.
(2) Frank, G.; Kostlin, H. *Appl. Phys. A: Mater. Sci. Process.* **1982**, *27*, 197−206.
(3) Yang, M.; Feng, J.; Li, G.; Zhnag, Q. *J. Cryst. Growth* **2008**, *310*, 3474−3477.
(4) Abe, I.; Ishiyama, N. *J. Mater. Sci.* **2006**, *41*, 7580−7584.
(5) Yan, L. T.; Schropp, R. E. I. *Thin Solid Films* **2012**, *520*, 2096−2101.
(6) Gupta, R.K.; Ghosh, K.; Mishra, S. R.; Khol, P.K. *Appl. Surf. Sci.* **2007**, *253*, 9422−9425.
(7) Sung, Y.-M.; Han, D.-W. *Vacuum* **2008**, *83*, 161−165.
(8) van Hest, M. F. A. M.; Dabney, M. S.; Perkins, J. D.; Ginley, D. S.; Taylor, M. P. *Appl. Phys. Lett.* **2005**, *87*, 032111.
(9) Sánchez-Marcos, J.; Ochando, I. M.; Escobar-Galindo, R.; Martínez-Morillas, R.; Prieto, C. *Phys. Status Solidi A* **2010**, *207*, 1549−1553.
(10) Kim, J. I.; Ji, K. H.; Jang, M.; Yang, H.; Choi, R.; Jeong, J. K. *ACS Appl. Mater. Interfaces* **2011**, 3, 2522−2528.
(11) Ye, L. W.; Gougousi, T. *ACS Appl. Mater. Interfaces* **2013**, *5*, 8081−8087.
(12) Hoffmann, M.; Kopka, P.; Voges, E. *IEEE J. Sel. Top. Quantum Electron.* **51999**, *5*, 46−51.
(13) Tanabe, T.; Notomi, M.; Mitsugi, S.; Shinya, A.; Kuramochi, E. *Opt. Lett.* **2005**, *30*, 2575−2577.
(14) Liu, M. Y.; Chen, E.; Chou, S. *Appl. Phys. Lett.* **1994**, *65*, 887−889.
(15) Sharma, A. K.; Logofatu, P. C.; Mayberry, C. S.; Brueck, S. R. J.; Islam, N. E. *J. Appl. Phys.* **2007**, *101*, 104914.
(16) Mohammadi, M. R.; Cordero-Cabrera, M. C.; Fray, D. J.; Ghorbani, M. *Sens. Actuators, B* **2006**, *120*, 86−95.
(17) Studenikin, S. A.; Golego, N.; Cocivera, M. *J. Appl. Phys.* **1998**, *84*, 5001−4.
(18) Moazzami, K.; Murphy, T. E.; Phillips, J. D.; Cheung, M. C.-K.; Cartwright, A. N. *Semicond. Sci. Technol.* **2006**, *21*, 717−723.
(19) Barzola-Quiquia, J.; Esquinazi, P.; Villafuerte, M.; Heluani, S. P.; Pöppl, A.; Eisinger, K. *J. Appl. Phys.* **2010**, *108*, 073530.
(20) Comedi, D.; Heluani, S. P.; Villafuerte, M.; Arce, R. D.; Koropecki, R. R. *J. Phys.: Condens. Matter* **2007**, *19*, 486205.
(21) Klementiev, K. V. *J. Phys. D: Appl. Phys.* **2001**, *34*, 209−217.
(22) Ankudinov, A. L.; Ravel, B.; Rehr, J. J.; Conradson, S. D. *Phys. Rev. B* **1998**, *58*, 7565−7576.
(23) Rehr, J. J.; Albers, R. C. *Rev. Mod. Phys.* **2000**, *72*, 621−654.
(24) van der Pauw, L. J. *Philips Res. Rep.* **1958**, *13*, 1−9.
(25) Marezio, M. *Acta Crystallogr.* **1966**, *20*, 723−728.
(26) Rodríguez-Carvajal, J. *Physica B* **1921993**, *192*, 55−69.
(27) Nadaud, N.; Lequeux, N.; Nanot, M.; Jové, J.; Roisnel, T. *J. Solid State Chem.* **1998**, *135*, 140−148.
(28) Niu, M.; Cheng, D.; Huo, L.; Shao, X. *J. Alloys Compd.* **2012**, *539*, 221−226.
(29) Liu, X. D.; Jiang, E. Y.; Li, Z. Q.; Song, Q. G. *Appl. Phys. Lett.* **2008**, *92*, 252104.
(30) Ravel, B.; Stern, E.A. *Physica B* **1995**, *208&209*, 316−318.
(31) Verdinski, R.V.; Kraizman, V. L.; Novakovich, A. A.; Demekhin, Ph. V.; Urazhdin, S. V. *J. Phys.: Condens. Matter* **1998**, *10*, 9561−9580.
(32) Mastelaro, V.R.; Mesquita, A.; Neves, P.P.; Michalowicz, A.; Bounif, M.; Pizani, P.S.; Joya, M. R.; Eiras, J.A. *J. Appl. Phys.* **2009**, *105*, 033508.
(33) Holgado, J. P.; Caballero, A.; Espinos, J.P.; Morales, J.; Jimenez, V. M.; Justo, A.; Gonzalez-Elipe, A. R. *Thin Solid Films* **2000**, *377-378*, 460−466.
(34) Parent, Ph.; Dexpert, H.; Tourillon, G.; Grimal, J. M. *J. Electrochem. Soc.* **1992**, *139*, 282−285.
(35) Tauc, J. Optical Properties of Amorphous Semiconductors. In *Amorphous and Liquid Semiconductors*; Tauc, J., Ed.; Plenum: London, 1974; pp 159−312.
(36) Weiher, R. L.; Ley, R. P. *J. Appl. Phys.* **1966**, *37*, 299−301.
(37) Pérez-Pacheco, A.; Prieto, C.; Castañeda-Guzmán, R.; García-López, J. *Thin Solid Films* **2009**, *517*, 5415−5418.
(38) Yan, L. T.; Rath, J. K.; Schropp, R. E. I. *Appl. Surf. Sci.* **2011**, *257*, 9461−9465.
(39) Clark, A.H. Optical Properties of Polycrystalline Semiconductor Films. In *Polycrystalline and Amorphous Thin Films and Devices*; Kazmerski, L.L., Ed.; Academic Press: New York, 1980; pp 135−142.
(40) Szczyrbowski, J.; Czapla, A. *Thin Solid Films* **1977**, *46*, 127−137.
(41) Baban, C.; Rusu, G. I. *Appl. Surf. Sci.* **2003**, *211*, 6−12.
(42) Cody, C. D.; Tiedje, T.; Abeles, B.; Brooks, B.; Goldstein, Y. *Phys. Rev. Lett.* **1981**, *47*, 1480−1483.
(43) Blood, P.; Orton, J. W. *The Electrical Characterization of Semiconductors: Majority Carriers and Electron States*; Academic Press: London, 1992, pp 19−25.
(44) Bowers, J. W.; Upadhyaya, H. M.; Nakada, T.; Tiwari, A. N. *Sol. Energy Mater. Sol. Cells* **2010**, *94*, 691−696.
(45) Shigesato, Y.; Takaki, S.; Haranoh, T. *J. Appl. Phys.* **1992**, *71*, 3356−3364.
(46) O'Dwyer, C.; Szachowicz, M.; Visimberga, G.; Lavayen, V.; Newcomb, S. B.; Sotomayor-Torres, C. M. *Nat. Nanotechnol.* **2004**, *4*, 239−244.
(47) Nguyen, P.; Ng, H. T.; Yamada, T.; Smith, M. K.; Li, J.; Han, J.; Meyyappan, M. *Nano Lett.* **2004**, *4*, 651−657.
(48) Seeger, K. *Semiconductor Physics: An Introduction*; Springer Verlag: Berlin, 2002;l pp 1−525.
(49) Yang, Z.; Gao, S.; Li, T.; Liu, F.-Q.; Ren, Y.; Xu, T. *ACS Appl. Mater. Interfaces* **2012**, *4*, 4419−4427.
(50) Chandiran, A. K.; Yella, A.; Stefik, M.; Heiniger, L.-P.; Comte, P.; Nazeeruddin, M. K.; Grätzel, M. *ACS Appl. Mater. Interfaces* **2013**, *5*, 3487−3493.